



**HAL**  
open science

## Poroelasticity of the Callovo–Oxfordian Claystone

Malik Belmokhtar, Pierre Delage, Siavash Ghabezloo, Anh Minh A.M. Tang,  
Hamza Menaceur, Nathalie Conil

► **To cite this version:**

Malik Belmokhtar, Pierre Delage, Siavash Ghabezloo, Anh Minh A.M. Tang, Hamza Menaceur, et al.. Poroelasticity of the Callovo–Oxfordian Claystone. *Rock Mechanics and Rock Engineering*, 2017, 50 (4), pp.871 - 889. 10.1007/s00603-016-1137-3 . hal-01515962

**HAL Id: hal-01515962**

**<https://enpc.hal.science/hal-01515962>**

Submitted on 28 Apr 2017

**HAL** is a multi-disciplinary open access archive for the deposit and dissemination of scientific research documents, whether they are published or not. The documents may come from teaching and research institutions in France or abroad, or from public or private research centers.

L'archive ouverte pluridisciplinaire **HAL**, est destinée au dépôt et à la diffusion de documents scientifiques de niveau recherche, publiés ou non, émanant des établissements d'enseignement et de recherche français ou étrangers, des laboratoires publics ou privés.

## Poroelasticity of the Callovo-Oxfordian claystone

1 *Malik Belmokhtar<sup>1</sup>, Pierre Delage<sup>1</sup>, Siavash Ghabezloo<sup>1</sup>, Anh-Minh Tang<sup>1</sup>, Hamza Menaceur<sup>1,3</sup>, Nathalie Conil<sup>2</sup>*

2  
3  
4 <sup>1</sup>*Ecole des Ponts ParisTech, Laboratoire Navier/CERMES, 6-8 av. B. Pascal, F77455 Marne la Vallée, France*

5 <sup>2</sup>*Andra, Bure, France*

6  
7 <sup>3</sup>*Now at LEMTA, Université de Lorraine, Nancy, France*

8  
9 **Corresponding author :** Malik Belmokhtar  
10 E-mail : [malik.belmokhtar@enpc.fr](mailto:malik.belmokhtar@enpc.fr)  
11 Phone : 00 33 (0)1 64 15 35 39  
12

### 13 14 15 **Abstract**

16  
17 This work is devoted to an experimental investigation of the poroelastic behaviour of the Callovo-Oxfordian  
18 (COx) claystone, a potential host rock for the deep underground repository of high-level radioactive waste  
19 in France. Drained, undrained, pore pressure loading and unjacketed tests were carried out in a specially  
20 designed isotropic compression cell to determine the poroelastic parameters of fully saturated specimens.  
21 Great care was devoted to the saturation procedure and very small loading rates were used to ensure full  
22 drainage conditions in drained and pore pressure tests (0.5 kPa/min) and in the unjacketed test (2 kPa/min).  
23 High precision strain measurements were performed by ensuring direct contact between the LVDTs' stems  
24 and the specimen, allowing to stay within the elastic domain during the tests. A set of poroelastic parameters  
25 was determined on two specimens under different confining stresses and a very good compatibility between  
26 the data of different tests was found, giving confidence in the data obtained. The unjacketed test provided  
27 a directly reliable measurement of the unjacketed modulus ( $K_s = 21.73$  GPa) that was afterwards confirmed  
28 by an indirect evaluation that shows the non-dependency of  $K_s$  with respect to the stress level. A stress  
29 dependent Biot's coefficient  $b$  was found equal to 0.87 and 0.91 under 10 MPa and 8 MPa of Terzaghi  
30 effective stress respectively. An analysis in the framework of transverse isotropic poroelasticity provided  
31 the anisotropic Biot effective stress coefficients  $b_1$  (perpendicular to bedding) and  $b_2$  (parallel to bedding)  
32 with a higher value in the direction parallel to bedding. These parameters are that of specimens cored and  
33 trimmed in the laboratory. Given the high sensitivity of the claystone to damage, the values obtained here,  
34 which could be overestimated by damage, are to be compared with values that could be get from in-situ  
35 testing.  
36  
37  
38  
39  
40  
41  
42  
43  
44  
45  
46  
47  
48

49  
50  
51  
52 **Keywords:** Claystone, poroelasticity, Biot's coefficient, unjacketed modulus, isotropic compression cell.  
53  
54  
55  
56  
57  
58  
59  
60  
61  
62  
63  
64  
65

## 1. Introduction

1 A possible host rock for geological radioactive waste disposal in France is the Callovo-  
2 Oxfordian (COx) claystone, a sedimentary clayey rock from the Paris basin deposited 155 million  
3 years ago into a 150 m thick layer over a layer of Dogger limestone and covered by a layer of  
4 Oxfordian limestone. Detailed investigations on the properties of the COx claystone are carried  
5 out in the Underground Research Laboratory (URL) managed by Andra, the French agency for the  
6 management of radioactive waste, close to the village of Bure in Eastern France. The URL is  
7 located at a depth of 490 m, at which the clay fraction in the claystone is maximum and close to  
8 50%. A detailed investigation of the in-situ state of stress in the Bure URL was conducted by  
9 Wileveau *et al.* (2007), providing the following stress values: vertical total stress  $\sigma_V = 12.7$  MPa  
10 (lithostatic), major horizontal stress  $\sigma_H = 12.7-14.8$  MPa, minor horizontal stress  $\sigma_h = 12.4$  MPa  
11 and pore pressure  $u = 4.9$  MPa. Typical characteristics of the COx claystone are a very low  
12 permeability (in order of  $10^{-20}$  m<sup>2</sup>) (Escoffier, 2002; Davy *et al.*, 2007; Zhang, 2011 ; Menaceur *et*  
13 *al.*, 2015a, 2015b), a high sorption capacity for radionuclides and a low diffusion coefficient  
14 resulting in very slow solute transfer.

15 To optimize the design of the galleries and disposal cells of a possible geological waste  
16 repository in the COx claystone, various investigations have been carried out to explore its  
17 hydromechanical behaviour (Chiarelli, 2000; Chiarelli *et al.*, 2003; Zhang & Rothfuchs, 2004;  
18 Hoxha *et al.*, 2007; Hu *et al.*, 2013; Menaceur *et al.*, 2015a, 2015b). As quoted by Menaceur *et*  
19 *al.* (2015b), the variability observed in published data can be linked to the different experimental  
20 procedures adopted by the different research groups involved, with respect to the state of saturation  
21 of the specimens and to the drainage conditions imposed during triaxial testing. The significant  
22 sensitivity of claystones to changes in water content has been observed by Zhang *et al.* (2012),  
23 Pham *et al.* (2007), Valès *et al.* (2004), Zhang and Rothfuchs (2004) and Chiarelli *et al.* (2003),  
24 with larger strength at lower degrees of saturation. The importance of adopting short drainage  
25 length to ensure good saturation (under stress conditions close to the in-situ ones) within a  
26 reasonable period of time (no longer than one week) has been demonstrated by Monfared *et al.*  
27 (2011a). Actually, short drainage length ensured satisfactory drainage conditions with  
28 homogeneous pore pressure field within the specimens, allowing to investigate the intrinsic  
29 response of low porosity specimens through fully drained tests with no excess pore pressure. In  
30 this regard, Monfared *et al.* (2011a) developed a new hollow cylinder triaxial apparatus with a  
31 drainage length of 10 mm. Hu *et al.* (2014) also tested small sized triaxial specimens (20 mm in  
32 diameter and 40 mm in height). The failure criteria obtained on COx specimens by Hu *et al.* (2013)

1 on fully saturated and fully drained specimens appeared to be compatible with that obtained on the  
2 hollow cylinder apparatus by Menaceur *et al.*, (2015b) on specimens of comparable porosity.  
3 Imperfect saturation and drainage conditions are known to over-estimate the mechanical  
4 characteristics (larger stiffness and larger failure stress).  
5

6 Rather few studies addressed the poroelastic response of claystones (Vincké *et al.*, 1998;  
7 Escoffier, 2002; Bemmer *et al.*, 2004; Noiret *et al.*, 2010). Existing data show that various values of  
8 the modulus of the solid phase  $K_s$  have been found, resulting in a large range of possible values of  
9 the Biot coefficient  $b$ , between 0.33 and 0.95 (Escoffier, 2002). This variability is due to several  
10 reasons: natural variability of the samples (mineralogy, water content, porosity...), coring and  
11 trimming procedures, testing protocols adopted with respect to saturation and drainage  
12 procedures... Currently, the  $b$  reference value adopted by Andra in numerical calculations is most  
13 often taken equal to 0.6 (Gens *et al.*, 2007; Charlier *et al.*, 2013). However, because of these  
14 uncertainties, it seems hence necessary to further investigate the poro-elastic behaviour of the COx  
15 claystone so as to provide more reliable values of the poro-elastic parameters and to reduce their  
16 variability for poro-elastic calculations. To do so, a special isotropic compression cell developed  
17 by Tang *et al.* (2008) and adapted by Mohajerani *et al.* (2012) was used and further developed in  
18 this work. In this device, a reduced drainage length (10 mm) is ensured by using a 10 mm thick  
19 specimen drained at bottom. A high precision local strains measurements device was developed to  
20 allow a precise determination of the poro-elastic parameters of the Callovo-Oxfordian claystone  
21 that were investigated along various hydromechanical paths.  
22  
23  
24  
25  
26  
27  
28  
29  
30  
31  
32  
33  
34  
35

## 36 **2. Poroelastic framework**

37  
38 The Callovo-Oxfordian claystone is a saturated porous medium in which the solid phase is  
39 made up of various components that will be described in more details later on. This section  
40 successively recalls the fundamentals of poroelasticity of fully saturated porous media, first in  
41 isotropic conditions and then in the case of transverse isotropy, a case more adapted to sedimentary  
42 soils and rocks. The investigation carried out here is based on the use of an isotropic compression  
43 cell providing a hydrostatic stress state.  
44  
45  
46  
47  
48  
49

50 The changes in volumetric strain  $\varepsilon_v$  ( $\varepsilon_v = \varepsilon_1 + \varepsilon_2$ ) in which  $\varepsilon_1$  and  $\varepsilon_2$  are the strains along the  
51 axial direction 1 and the radial direction 2, respectively with respect to changes in total stress and  
52 pore pressure will be monitored during the tests. To do so, one first defines the Lagrangian porosity  
53 of a porous medium by the ratio of the pore volume  $V_\phi$  to the initial total volume  $V_0$  ( $\phi = V_\phi/V_0$ ).  
54 The volumetric strain is given by  $\varepsilon_v = -dV/V_0$ . Under changes in isotropic total stress  $\sigma$  (positive  
55  
56  
57  
58  
59  
60  
61  
62  
63  
64  
65

in compression), the volumetric behaviour of a saturated sample depends on the changes in pore fluid pressure  $u$  and in differential stress  $\sigma_d = \sigma - u$ , also called Terzaghi effective stress.

## 2.1. Isotropic poroelasticity

The poroelastic expressions of the changes in total volume  $V$  and in pore volume  $V_\phi$  with respect to changes in differential pressure  $\sigma_d$  and pore pressure  $u$  are defined by four compression modulus  $K_d, K_s, K_p, K_\phi$  according to the following relations:

$$-\frac{dV}{V_0} = \frac{1}{K_d} d\sigma_d + \frac{1}{K_s} du \quad (1)$$

$$-\frac{dV_\phi}{V_{\phi_0}} = \frac{1}{K_p} d\sigma_d + \frac{1}{K_\phi} du \quad (2)$$

These moduli are defined by the following relations:

$$\frac{1}{K_d} = -\frac{1}{V_0} \left( \frac{\partial V}{\partial \sigma_d} \right)_u, \quad \frac{1}{K_p} = -\frac{1}{V_{\phi_0}} \left( \frac{\partial V_\phi}{\partial \sigma_d} \right)_u \quad (3)$$

$$\frac{1}{K_s} = -\frac{1}{V_0} \left( \frac{\partial V}{\partial u} \right)_{\sigma_d}, \quad \frac{1}{K_\phi} = -\frac{1}{V_{\phi_0}} \left( \frac{\partial V_\phi}{\partial u} \right)_{\sigma_d} \quad (4)$$

Note that these relations could also be written in terms of compressibility coefficients  $c_i$  with  $c_i = 1/K_i$ .

The drained bulk modulus  $K_d$  and the modulus  $K_p$  in equation (1) are obtained by running an isotropic drained compression test in which the confining stress is increased while keeping the pore pressure constant and while monitoring the changes in total volume  $V$  and pore volume  $V_\phi$ , respectively.

The parameters of equation (2) are determined by running an unjacketed compression test, in which equal increments of confining stress and pore pressure are simultaneously applied to the sample, keeping constant the differential stress  $\sigma_d$ . The changes in sample volume with respect to changes in pressure provide the unjacketed modulus  $K_s$ . The changes in pore volume with respect to changes in pressure theoretically provide the unjacketed pore modulus  $K_\phi$ . Note however that the experimental evaluation of this parameter is quite difficult, if not impossible, since the fluid volume exchanged during the test and monitored through the pressure volume controller is significantly affected by the fluid compressibility and the deformation of the both the pressure volume controller and the drainage system (Ghabezloo *et al.*, 2008).

As quoted by Detournay and Cheng (1993), during an unjacketed test, a specimen of ideal porous material, homogeneous and isotropic at the micro-scale, would deform as if all pores were filled with the solid phase, resulting in a uniform volumetric strain for both the skeleton and the solid phase. In such a case,  $K_\phi = K_s = K_m$ , where  $K_m$  is the bulk modulus of the single solid constituent of the ideal porous material. This is why the unjacketed modulus  $K_s$  is also called the solid phase modulus in the literature. However, since the COx claystone is a micro-heterogeneous material in which the solid phase is composed of various minerals with distinct moduli, the expression of unjacketed modulus is preferred for  $K_s$ . In fact, the modulus  $K_s$  is some kind of weighted average of the bulk moduli of the constituents, the nature of which is not exactly known. However, Ghabezloo and Sulem (2009) evaluated the unjacketed modulus of the Rothbach sandstone using Hill's (1952) average formula and observed good accordance with the experimental data. The relation between the modulus  $K_\phi$  and the material properties appeared to be quite complex and the  $K_\phi$  value is generally not bounded by the elastic moduli of the solid components (Berryman, 1992). However, the assumption  $K_s = K_\phi$  is generally adopted in the literature in numerical simulations.

As shown by Zimmerman *et al.* (1986), based on Betti's reciprocal theorem, the following relation holds between the elastic moduli  $K_p$ ,  $K_d$  and  $K_s$ :

$$\frac{1}{K_p} = \frac{1}{\phi_0} \left( \frac{1}{K_d} - \frac{1}{K_s} \right) \quad (5)$$

Equation (1) can be rewritten in the following form to find the expression of Biot effective stress variation  $d\sigma' = d\sigma - bdu$ :

$$d\varepsilon_v = -\frac{dV}{V_0} = \frac{1}{K_d} \left[ d\sigma - du + \frac{K_d}{K_s} du \right] = \frac{1}{K_d} (d\sigma - b du) \quad (6)$$

Biot effective stress coefficient  $b$  is thus defined by:

$$b = 1 - \frac{K_d}{K_s} \quad (7)$$

Expression (6) shows that a test in which pore pressure is changed under constant total stress ( $d\sigma = 0$ ) provides the following relation between the volume change and the pore pressure change:

$$d\varepsilon_v = -\frac{b}{K_s} du \quad (8)$$

Biot modulus  $H$  can thus be defined as follows:

$$\frac{1}{H} = \frac{1}{V_0} \left( \frac{\partial V}{\partial u} \right)_\sigma = \frac{b}{K_d} = \frac{1}{K_d} - \frac{1}{K_s} \quad (9)$$

Expression (9) shows that knowing the drained modulus  $K_d$ , the determination of  $H$  provides an indirect evaluation of both the Biot coefficient  $b$  and the unjacketed modulus  $K_s$ .

Using Eqs. (1), (2), (5) and (8) one can write the variation of the Lagrangian porosity ( $d\phi/\phi_0 = dV_\phi/V_{\phi_0}$ ) in the following form:

$$d\phi = -b d\varepsilon_v + \frac{1}{N} du ; \quad \frac{1}{N} = \frac{b}{K_s} - \frac{\phi_0}{K_\phi} \quad (10)$$

where  $N$  is the Biot's skeleton modulus that relates the changes in pore pressure and porosity when strains are held constant.

The undrained condition is defined as a condition in which the fluid mass is kept constant in the sample ( $dm_w = 0$  where  $m_w = \rho_w \phi$  is the fluid mass per unit volume of the porous sample). An undrained isotropic compression test is carried out in a triaxial/isotropic cell by closing the valves of the drainage system and by measuring the change in pore pressure  $u$  with respect to changes in isotropic compression stress  $\sigma$ . Two parameters can be determined, the undrained bulk modulus  $K_u$  and the Skempton coefficient  $B$  (Skempton, 1954), defined as follows:

$$B = \left( \frac{du}{d\sigma} \right)_{m_f}, \quad \frac{1}{K_u} = -\frac{1}{V_0} \left( \frac{dV}{d\sigma} \right)_{m_f} \quad (11)$$

The changes in water mass  $dm_w$  in undrained conditions is null, resulting in the relation  $dm_w = \phi d\rho_w + \rho_w d\phi = 0$ . The term  $d\phi$  is given by equation (10) and the change in water unit mass is given by expression  $d\rho_w/\rho_w = du/K_w$  (where  $K_w$  is the water modulus). Using these relations, one can find the following expression for the Skempton coefficient  $B$  (Skempton, 1954).

$$B = \frac{\left( \frac{1}{K_d} - \frac{1}{K_s} \right)}{\left( \frac{1}{K_d} - \frac{1}{K_s} \right) + \phi_0 \left( \frac{1}{K_w} - \frac{1}{K_\phi} \right)} \quad (12)$$

By replacing  $du = B d\sigma$  in equation (6) the following relation can be obtained for the undrained bulk modulus:

$$K_u = \frac{K_d}{1 - b B} \quad (13)$$

The experimental program followed here is based on the previous equations. It aims at characterizing the various poroelastic parameters by running different tests to examine the compatibility between the results obtained, in an aim to get satisfactory confidence in the experimental determination of the poroelastic parameters.

## 2.2. Transverse isotropic poroelasticity

The COx claystone is known as being transversely isotropic like many clayey sediments, with a preferential average orientation of the clay particles along a bedding plane that can be observed in scanning electron microscopy (e.g. Menaceur, 2014). The samples tested in this work have been cored perpendicular to the bedding planes. The anisotropic properties of the COx claystone have been detected in particular by Escoffier (2002), Chiarelli (2000), Andra (2005), Mohajerani *et al.*, (2012), Zhang *et al.* (2012). Typically, the axial stiffness is larger than radial one. Zhang *et al.*, (2012) performed a series of mini-compression tests on samples parallel and perpendicular to bedding planes under different relative humidities (RH). They observed a significant structural anisotropy reflected by a ratio of Young moduli  $E_2/E_1$  (with  $E_2$  and  $E_1$  parallel and perpendicular to bedding, respectively) varying between 1.6 and 1.9 (increasing with decrease of RH). The Young moduli measured at RH = 98% of are  $E_1 = 1.35$  GPa and  $E_2 = 2.22$  GPa, respectively. Note that these values are smaller than the values currently used in numerical simulations with  $E$  taken equal to 4 GPa (Gens *et al.*, 2007; Charlier *et al.*, 2013). As a consequence, an anisotropic response can be expected from the isotropic compression paths planned in this work, as observed by Noiret *et al.* (2010) on the Tournemire shale.

Anisotropic poroelasticity has been considered by several authors, including Thompson and Willis (1991), Detournay and Cheng (1993), Cheng (1997) and Zimmerman (2000). The generalized Hooke's law for a porous material is given by the relation  $\underline{\underline{\varepsilon}} = \underline{\underline{C}}^{-1}(\underline{\underline{\sigma}} - \underline{\underline{b}}u)$  (Cheng, 1997) where  $\underline{\underline{b}}$  is the Biot's coefficient tensor and  $\underline{\underline{C}}^{-1}$  the compliance tensor for a transverse isotropic material given by :

$$\underline{\underline{C}}^{-1} = \begin{pmatrix} \frac{1}{E_1} & \frac{-\nu_{12}}{E_1} & \frac{-\nu_{12}}{E_1} \\ \frac{-\nu_{12}}{E_1} & \frac{1}{E_2} & \frac{-\nu_{23}}{E_2} \\ \frac{-\nu_{12}}{E_1} & \frac{-\nu_{23}}{E_2} & \frac{1}{E_2} \end{pmatrix} \quad (14)$$

In the case of a transverse isotropic material submitted to an isotropic stress increment ( $d\sigma_1 = d\sigma_2 = d\sigma_3 = d\sigma$ ) the stress-strain relation can be written in the following form:

$$d\varepsilon_1 = \frac{1}{E_1}(d\sigma - b_1 du) - \frac{2\nu_{12}}{E_1}(d\sigma - b_2 du) \quad (15)$$

$$d\varepsilon_2 = -\frac{\nu_{12}}{E_1}(d\sigma - b_1 du) + \frac{(1 - \nu_{23})}{E_2}(d\sigma - b_2 du) \quad (16)$$

in which the  $x_1$  axis is taken perpendicular to bedding with  $x_2$  and  $x_3$  parallel to bedding.  $E_1$  is the Young modulus along direction  $x_1$  perpendicular to bedding and  $\nu_{12}$  the Poisson ratio in the  $(x_1, x_2)$  plane.  $E_2$  and  $\nu_{23}$  are the Young modulus and the Poisson ratio in the  $(x_2, x_3)$  plane, respectively. For symmetry reasons, the Young moduli and Poisson ratios verify the relation  $\nu_{12}/E_1 = \nu_{21}/E_2$ .

After Cheng (1997), the Biot coefficients  $b_1$  and  $b_2$  are defined by equations (15) and (16)

$$b_1 = 1 - \frac{M_{11} + 2M_{12}}{3K_s} \quad (17)$$

$$b_2 = 1 - \frac{M_{12} + M_{22} + M_{23}}{3K_s} \quad (18)$$

where,

$$M_{11} = \frac{E_1^2(1 - \nu_{23})}{E_1 - E_1\nu_{23} - 2E_2\nu_{12}^2} \quad (19)$$

$$M_{12} = \frac{E_2 E_1 \nu_{12}}{E_1 - E_1\nu_{23} - 2E_2\nu_{12}^2} \quad (20)$$

$$M_{22} = \frac{E_2(E_1 + E_2\nu_{12}^2)}{(1 + \nu_{23})(E_1 - E_1\nu_{23} - 2E_2\nu_{12}^2)} \quad (21)$$

$$M_{23} = \frac{E_2(E_1\nu_{23} + E_2\nu_{12}^2)}{(1 + \nu_{23})(E_1 - E_1\nu_{23} - 2E_2\nu_{12}^2)} \quad (22)$$

The combination of the different loading conditions considered here (drained, undrained, pore pressure changes and unjacketed conditions) allows writing the anisotropic modulus measured in each test from relations (15) and (16).

In the case of drained isotropic compression test where pore pressure is kept constant ( $du = 0$ ), the measured anisotropic moduli, called  $D_1$  and  $D_2$  in directions  $x_1$  and  $x_2$ , respectively, are given by the following relations :

$$\frac{1}{D_1} = \frac{d\varepsilon_1}{d\sigma} = \frac{1}{E_1}(1 - 2\nu_{12}) \quad (23)$$

$$\frac{1}{D_2} = \frac{d\varepsilon_2}{d\sigma} = -\frac{\nu_{12}}{E_1} + \frac{(1 - \nu_{23})}{E_2} \quad (24)$$

The measured anisotropic moduli in the case of the pore pressure test (change in pore pressure under constant confining pressure,  $d\sigma = 0$ ) are called  $H_1$  and  $H_2$  in directions  $x_1$  and  $x_2$  and are given by the following relations:

$$\frac{1}{H_1} = \frac{d\varepsilon_1}{du} = -\frac{b_1}{E_1} + 2\nu_{12} \frac{b_2}{E_1} \quad (25)$$

$$\frac{1}{H_2} = \frac{d\varepsilon_2}{du} = \frac{\nu_{12}}{E_1} b_1 - \frac{(1-\nu_{23})}{E_2} b_2 \quad (26)$$

In the same way, one can write the anisotropic undrained moduli that can be measured when running an undrained isotropic compression test. During this test, the relation between the increments of pore pressure and total stress is  $du = B d\sigma$ , where  $B$  is the Skempton coefficient. The undrained anisotropic moduli  $U_1$  and  $U_2$  in directions  $x_1$  and  $x_2$  are given by:

$$\frac{1}{U_1} = \frac{d\varepsilon_1}{d\sigma} = \frac{1}{E_1} ((1-b_1B) - 2\nu_{12}(1-b_2B)) \quad (27)$$

$$\frac{1}{U_2} = \frac{d\varepsilon_2}{d\sigma} = -\frac{\nu_{12}}{E_1} (1-b_1B) + \frac{(1-\nu_{23})}{E_2} (1-b_2B) \quad (28)$$

The unjacketed test (where  $d\sigma = du$ ) can also provide the unjacketed anisotropic moduli  $S_1$  and  $S_2$  in directions  $x_1$  and  $x_2$ , respectively, as follows:

$$\frac{1}{S_1} = \frac{d\varepsilon_1}{d\sigma} = \frac{1}{E_1} ((1-b_1) - 2\nu_{12}(1-b_2)) \quad (29)$$

$$\frac{1}{S_2} = \frac{d\varepsilon_2}{d\sigma} = -\frac{\nu_{12}}{E_1} (1-b_1) + \frac{(1-\nu_{23})}{E_2} (1-b_2) \quad (30)$$

This poroelastic framework can now be used to interpret the data obtained with the high precision isotropic compression cell.

### 3. Material and methods

#### 3.1. The Callovo-Oxfordian claystone

The mineralogical composition of the COx claystone and more specifically the clay and carbonate contents, vary with depth. The total porosity is estimated between 14% in carbonated levels and 19.5% in more argillaceous levels (Yven *et al.*, 2007). At the level of the Bure URL, the COx claystone is made up of a clay matrix (45-50% clay fraction) in which are embedded 20-30% carbonates, 20-30% quartz and a small fraction of feldspar. The clay fraction is composed of 10-24% mixed layer illite/smectite, 17-21% illite, 3-5% kaolinite, 2-3% chlorite (Gaucher *et al.*, 2004). The smectite fraction of the mixed layer illite/smectite is estimated between 50 and 70%. It provides to the COx claystone some swelling properties (e.g. Mohajerani *et al.*, 2012; Delage *et*

1  
2  
3  
4  
5  
6  
7  
8  
9  
10  
11  
12  
13  
14  
15  
16  
17  
18  
19  
20  
21  
22  
23  
24  
25  
26  
27  
28  
29  
30  
31  
32  
33  
34  
35  
36  
37  
38  
39  
40  
41  
42  
43  
44  
45  
46  
47  
48  
49  
50  
51  
52  
53  
54  
55  
56  
57  
58  
59  
60  
61  
62  
63  
64  
65

*al.*, 2014) and interesting self-sealing capabilities (Davy *et al.*, 2007; Zhang, 2011; Menaceur *et al.*, 2015b).

The specimens tested in this study (EST31912c and e) come from 80 mm diameter cores that were extracted at the depth of the Bure URL (490 m). Two specimens of 38 mm diameter and 10 mm height were cored by using a diamond core in the direction perpendicular to the bedding plane and cut at the required length by using a diamond saw. The water content was obtained by weighing the sample before and after oven drying at 105°C during 48 hours. The sample volume was determined by hydrostatic weighing to calculate the total connected porosity and the initial degree of saturation. The specimen EST31912c was tested immediately after coring. Its initial water content was equal to 7.45%, corresponding to a degree of saturation of 94.2%, considering a particle density of 2.70 g/cm<sup>3</sup> (Andra 2005). The specimen EST31912e, that was tested two months later, was preserved from evaporation by plunging it in a mix 70% paraffin 30% vaseline oil and wrapping it in plastic film. Its water content however decreased to 4.54% during the conservation period, corresponding to a degree of saturation of 67.8%. The initial characteristics of the two specimens tested are presented in Table 1. A suction measurement was carried out on some cuttings of specimen EST31912c by using a chilled mirror tensiometer (WP4, Decagon), providing a value of 19.7 MPa for a specimen with a degree of saturation of 94.2%. These data are representative of a good preservation of the specimen. They are in good compatibility with the water retention curves provided by Pham *et al.* (2007) and Wan *et al.* (2013). This measurement was unfortunately not carried out on specimen EST31912e.

### 3.2. Experimental device

The experimental device developed in this work is an extension of a system initially developed by Tang *et al.* (2008) to investigate the thermal behaviour of compacted bentonites. It was further developed by Mohajerani *et al.* (2012) to investigate thermal pressurization in the COx claystone. As shown in Figure 1, it is composed of a thermal isotropic compression cell connected to two pressure-volume controllers (PVC, GDS Brand) imposing pressures up to 60 MPa. Compared to previous works, the sample diameter was reduced to 38 mm in order to add a local system of axial and radial strains measurement by mean of LVDTs (Figure 1a). The short height of the sample (10 mm with drainage at bottom) results in a short drainage length that ensures a good saturation within a reasonable period of time and good drainage (see Monfared *et al.*, 2011a). Drainage was ensured by a thin geotextile on specimen EST31912c. To reduce the compressibility of the drainage system, the geotextile was replaced by a porous disk for specimen EST31912e. The difference between the two drainage systems (geotextile and porous disk) slightly affects the

1 measurement of the undrained parameters. A correction of the parasite effects of the pore volume  
2 of the drainage system is presented in the Appendix. Monfared (2011) checked the drainage  
3 performances of the geotextile under pressure. To insulate the sample from the confining fluid  
4 (silicone oil), a specially designed cylindrical neoprene membrane able to continuously envelop  
5 the top and lateral face of the sample was used, without using any piston or porous disk on the top  
6 of the sample. The membrane was tightly fixed to the bottom base by means of two O-rings.  
7  
8

9  
10 As shown in Figure 1-b, the cell was immersed in a temperature-controlled bath. Pore  
11 pressure changes in the sample were measured by a pressure transducer (0 to 75 MPa range) placed  
12 outside the bath to avoid any perturbation due to the temperature changes in the bath. The  
13 temperature of the bath was controlled with 0.1°C accuracy and measured by means of a  
14 thermocouple. One of the two ducts arriving at the sample bottom was connected to the pressure  
15 transducer whereas the other one was connected to the back pressure PVC. This PVC was carefully  
16 filled by demineralized and de-aired water.  
17  
18  
19  
20  
21  
22

### 23 **3.3. Strain measurement**

24  
25 The main improvement with respect to the device of Mohajerani *et al.* (2012) concerns the  
26 monitoring of the axial and radial strain by means of LVDTs, as shown in Figure 2. Given the  
27 stiffness of the COx claystone, with a Young modulus of about 4000-5600 MPa (Andra 2005;  
28 Gens *et al.*, 2007; Charlier *et al.*, 2013) and because of the small size of the sample, the  
29 displacements during compression are expected to be small (around 2 µm by MPa). To avoid any  
30 disturbance due to the neoprene membrane, direct contact between the LVDT stem and the  
31 specimen was ensured by piercing the membrane with a hole smaller in diameter than the stem.  
32 Good fluid tightness was ensured by putting a drop of neoprene glue on the membrane around the  
33 stem. Using this technique, displacement measurements were improved with a minimum accuracy  
34 of 0.1 µm corresponding to a strain of 10<sup>-5</sup>.  
35  
36  
37  
38  
39  
40  
41  
42  
43  
44

45 Figure 3 shows a comparison during an undrained compression test between the data of the  
46 radial LVDT in direct contact with the specimen through the membrane and that obtained by the  
47 axial one in contact with the membrane. Starting from an initial confining stress of 12 MPa with a  
48 back pressure of 4 MPa, the confining stress was increased with a loading rate of 20 kPa/min and  
49 maintained at 16.5 MPa during 13 hours. Afterwards, an unloading-reloading path up to a  
50 maximum pressure of 18.5 MPa was followed. Finally, the confining stress was decreased down  
51 to 12 MPa with a loading rate of 10 kPa/min. The comparison between the two measurements  
52 clearly shows that the LVDT in direct contact with the sample precisely follows all the loading  
53 and unloading phases, while the measurements made on the membrane do not detect the unloading  
54  
55  
56  
57  
58  
59  
60  
61  
62  
63  
64  
65

1 phases at the 18 and 26<sup>th</sup> hours. The loading sequence at 20h is also poorly monitored. This clearly  
2 shows the improvement provided by ensuring a direct contact of the LVDT stem with the specimen  
3 through the membrane.

#### 4 **3.4. Saturation phase**

5  
6  
7 As demonstrated in swelling soils (e.g. Delage *et al.* (2007) and applied by Monfared *et al.*  
8 (2011a) on the Opalinus clay and Mohajerani *et al.* (2011) and Menaceur *et al.* (2015a, 2015b) on  
9 the COx claystone, it is mandatory to saturate swelling soils and clay rocks under stress conditions  
10 close to in-situ one to minimize possible swelling and damage. To do so, the ducts and the  
11 geotextile were kept dry during the sample setup to avoid any contact of the sample with water.  
12 Once the sample placed on the base with the membrane put around and the cell placed and filled  
13 with the confining fluid (oil), vacuum was applied through the valve located close to the pressure  
14 transducer (valve V2 in Figure 2) so as to evacuate any trapped air between the membrane and the  
15 sample. Then, the confining pressure was increased to 8 MPa, a value close to the in-situ Terzaghi  
16 effective stress. The drainage system under vacuum was afterwards filled with de-aired water  
17 through valve V2 while valve V1 was kept closed, ensuring good saturation of the drainage system.  
18 Finally, the confining stress and pore pressure were simultaneously increased up to 12 MPa and  
19 4 MPa respectively at a rate of 100 kPa/min to reach stress conditions close to in-situ.  
20  
21  
22  
23  
24  
25  
26  
27  
28  
29  
30

31 Figure 4a shows the water exchange (i.e. the ratio of injected water  $\Delta V_w$  monitored by the  
32 PVC with respect to the initial sample volume  $V_0$ ) together with the volumetric strains measured  
33 by the LVDTs in tests EST31912c. The sample exhibit a small swelling (0.05%, at the limit of the  
34 precision of the PVC) with axial swelling larger than radial swelling. The monitoring of water  
35 exchanges does not seem to be satisfactory during the first day, but a good compatibility of the  
36 volume changes with water exchanges is observed after one day.  
37  
38  
39  
40  
41  
42

43 The response of the axial LVDT is not satisfactory for sample EST31912e (Figure 4b) and  
44 no volume change could be calculated from local strain measurement. The radial strain stabilizes  
45 after one and a half day, like in sample EST31912c, but at a value significantly larger, a possible  
46 effect of the smaller initial degree of saturation.  
47  
48  
49

50 A possible reason of the significant difference in the swelling response is the difference in  
51 initial degree of saturation, with values of 94.2% and 67.8% for samples EST31912c and  
52 EST31912e, respectively. Similar observations were made by Menaceur (2014) when testing in  
53 the oedometer two samples of COx samples with degrees of saturations of 77% and 91% and by  
54 Ewy (2015) who found larger swelling in shales and claystones with lower partial saturation.  
55  
56  
57  
58  
59  
60  
61  
62  
63  
64  
65

Indeed, loss of water (drying) in clayey rocks results in damage and micro-cracks that enhance swelling.

### 3.5. Loading rates

When performing a drained compression test, the pore pressure field should remain homogeneous with negligible changes in pore pressure (Gibson and Henkel, 1954). Homogeneity of the pore pressure field is also mandatory when performing an unjacketed test or an undrained compression test. In practice, pore pressure can only be controlled at the sample borders connected with the drainage system. This occurs at the bottom of the 10 mm high cylindrical specimen in the isotropic compression tests carried out here. In all cases, pore pressure homogeneity can be ensured if a sufficiently low stress rate is adopted. The loading rates depends on the sample permeability, drainage length, material's stiffness and of the nature of the test carried out. It is impossible to have a perfectly homogeneous pore pressure distribution, however a loading rate can be considered as satisfactory for a given loading path when the generated pore pressure heterogeneity inside the sample has a negligible influence on the measured strains and consequently on the evaluated poroelastic parameters.

A loading rate of 0.5 kPa/min was adopted for the drained compression test, like in Sultan *et al.* (2000) on the Boom clay and Monfared *et al.* (2011a) who used a hollow cylinder triaxial cell with 10 mm drainage length on Boom clay and Opalinus clay. This value was validated by poroelastic numerical simulations performed to investigate pore pressure homogeneity and the effect of the loading rate on the measurement of the moduli in all the tests performed, including that in which pore pressure was changed under constant total stress. A loading rate of 2 kPa/min appeared to be satisfactory for the unjacketed test.

### 3.6. Correction of drainage system effect for the undrained experiments

Undrained compression tests are run by increasing the confining pressure while all valves of the drainage system are closed. The confining pressure variation results in a simultaneous change of the sample pore pressure. The measurement of the pore pressure change by the pressure transducer inevitably requires some fluid mass exchange between the pore volumes of the sample and of the drainage system. The loading rate should thus be slow enough to ensure pore pressure equilibrium between these pore volumes. Therefore, the undrained condition ( $\Delta m_w = 0$ ) cannot be ensured in the pore volume of the sample only, it is actually imposed in the larger volume including the pore volumes of both the specimen and the drainage and pore pressure measurement system. This artefact induces some error in the measured undrained parameters due to the compressibility

of the drainage system and of the fluid filling it. A correction method should thus be applied to the measured parameters.

Wissa (1969) and Bishop (1976) were the first who proposed a correction method for the effect of the drainage system on the results of an undrained compression test. It was then extended by Ghabezloo and Sulem (2009, 2010) to correct the pore pressure and volumetric strain in an undrained heating test. This correction method has been applied, with some additional terms to take into account the presence of geotextile in the drainage system, to the results of experiments performed on Opalinus clay (Monfared *et al.*, 2011a) and COx claystone (Mohajerani *et al.*, 2012). The correction method is presented in the Appendix along with a parametric study on the effects of various parameters.

#### 4. Experimental program and results

Various cycles in isotropic stress have been carried out to determine independently the five following poroelastic parameters:

- Theunjacketed modulus  $K_s$ , determined by running an unjacketed compression test in which pore pressure and confining pressure are simultaneously increased, keeping the Terzaghi effective stress constant.
- The drained bulk modulus  $K_d$ , determined by running a drained isotropic compression test in which the confining pressure is increased under constant pore pressure.
- The Biot modulus  $H$ , determined by running a “pore pressure” test in which pore pressure is changed under constant total stress.
- The undrained bulk modulus  $K_u$ , determined by running an undrained isotropic compression test.
- The Skempton coefficient  $B = \Delta u / \Delta \sigma$  determined by measuring the increase in pore pressure  $\Delta u$  resulting from an undrained isotropic compression under an increment of total stress  $\Delta \sigma$ .

The experimental program was carried out under initial isotropic Terzaghi effective stresses of 10 MPa for test EST31912c and 8 MPa for test EST31912e.

##### 4.1. Unjacketed compression test

As seen in Eq. 1, a direct method to estimate the unjacketed modulus  $K_s$  consists in performing an unjacketed compression test by simultaneously increasing the confining pressure and the pore pressure ( $\Delta \sigma = \Delta u$ ), hence keeping the differential (Terzaghi effective) stress constant. For proper determination of  $K_s$ , a good precision in strain measurements is necessary.

Moreover, the very low permeability of the COx claystone makes unjacketed compression tests quite long because of the small loading rate necessary to ensure a homogeneous pore pressure field. The results of an unjacketed test carried out with the high precision device of Figure 1 on sample EST31912c at a loading rate of 2 kPa/mn are presented in Figure 5. The isotropic confining pressure was increased from 14 MPa to 16 MPa and the pore pressure from 4 MPa to 6 MPa, keeping a constant value of the Terzaghi stress of 10 MPa. The data are presented in terms of change in axial and radial strain with respect to isotropic confining pressure. At maximum confining pressure (16 MPa) a maximum axial strain of 0.012% that corresponds to a displacement value of 0.8  $\mu\text{m}$  (indicating the good performance of the local strain measurement) is measured. A significantly anisotropic response is observed with radial strains ( $\varepsilon_2$ , parallel to bedding) significantly smaller than axial ones ( $\varepsilon_1$ , perpendicular to bedding) and a ratio  $\varepsilon_2/\varepsilon_1$  equal to 5.7. The isotropic equivalent unjacketed modulus obtained is equal to 21.73 GPa, corresponding to a compressibility coefficient  $c_s$  ( $1/ K_s$ ) equal to  $0.046 \text{ GPa}^{-1}$ .

## 4.2. Undrained compression test

The undrained compression test is aimed at providing the undrained bulk modulus  $K_u$  and the Skempton  $B$  coefficient. Both parameters are related by equation (13) and were determined along an unloading/reloading path to make sure to keep staying in the elastic domain.

### 4.2.1. Skempton coefficient

Figure 6 presents the changes in pore pressure as a function of the confining pressure during an undrained test run on sample EST31912c by unloading the confining stress from 14 MPa down to 12.8 MPa. The response is quite linear and the slope provides a measured value of the Skempton coefficient  $B^{meas} = 0.63$ .

The correction (see Appendix) provides a corrected value  $B^{corr} = 0.84$ , with a difference compared to  $B^{meas}$  of about 25%, mostly due to the compressibility of water and to the large dead volume of the drainage system (geotextile). This corrected Skempton coefficient  $B^{corr}$  is equal to that found in the COx claystone by Mohajerani *et al.* (2013) in a hollow cylinder triaxial cell. These authors demonstrated that  $B = 0.84$  indicated a good saturation of the specimen.

Unfortunately, a leak occurred during the test on sample EST31912e and no  $B$  value could be obtained.

#### 4.2.2. Undrained bulk modulus ( $K_u$ )

1 The measurement of the undrained bulk modulus was achieved on both samples with axial  
2 and radial strains monitored. Only one unloading sequence from 13.9 down to 12.8 MPa was  
3 carried out in the test on sample EST31912c. Four cycles were performed between 12 MPa and  
4 11 MPa in the test on sample EST31912e, as seen in Figure 7 showing the changes in radial, axial  
5 and volumetric strains with respect to the confining pressure for both tests.  
6  
7  
8  
9

10 Linear responses with clear anisotropy are again observed in axial and radial strains with an  
11 anisotropy ratio of 3.7 and 3.5 for tests EST31912c and EST31912e, respectively. This ratio is  
12 quite different compared to that observed in the unjacketed test. Load cycles provide a satisfactory  
13 reversible response in the test on sample EST31912e (Figure 7b). The maximum strain measured  
14 by the radial LVDTs is equal to 0.003% ( $10^{-5}$ , say a displacement of 0.52  $\mu\text{m}$ ), and that measured  
15 by axial LVDT is 0.011%, say a displacement of 1.09  $\mu\text{m}$ ), confirming the high precision  
16 performance of the monitoring of the local strains.  
17  
18  
19  
20  
21  
22

23 The measured undrained moduli are  $K_u^{mes} = 7090$  MPa for test EST31912c and  $K_u^{mes} = 6480$   
24 MPa for test EST31912e and they correspond to corrected values  $K_u^{cor} = 12420$  MPa and  
25  $K_u^{cor} = 10930$  MPa, respectively. The significantly lower measured values are due to the high ratio  
26 between the volume of the drainage system and the sample volume ( $V_L/V$ ) (see Appendix). The  
27 lower value of the undrained bulk modulus in test EST31912e compared to that in test EST31912c  
28 is due to the lower applied Terzaghi effective stress. The relatively good correspondence between  
29 the two values provides a good confidence in the  $K_u$  values obtained.  
30  
31  
32  
33  
34  
35  
36

#### 37 4.3. Drained compression test

38 The drained compression test conducted to determine the drained bulk modulus  $K_d$  was  
39 carried out by keeping the pore pressure constant ( $du = 0$ ) by connecting valve V1 (Figure 1-b) to  
40 the PVC controlling the pore pressure ( $u = 4$  MPa). A loading rate of 0.5 kPa/min was adopted to  
41 ensure satisfactory drained conditions with the drainage length of 10 mm. Thanks to the accuracy  
42 of the strain measurements, small stress cycles of only 500 kPa were applied, a small enough range  
43 to stay within the elastic domain.  
44  
45  
46  
47  
48  
49  
50

51 Three drained unloading-reloading cycles were performed, one on sample EST31912c  
52 (between 14 MPa and 13.5 MPa) and two on sample EST31912e (between 12 MPa and 11.6 MPa  
53 and between 12 MPa and 11.4 MPa). Like in previous tests, the response in axial and radial strain  
54 indicates some anisotropy (Figure 8) with smaller radial strains with ratios  $\epsilon_1/\epsilon_2$  of 2.3 and 2.4  
55 for samples EST31912c and EST31912e, respectively. The good repeatability observed in the two  
56 cycles carried out on sample EST31912e (Figure 8b) provides good confidence in the results. One  
57  
58  
59  
60  
61  
62  
63  
64  
65

also observes the stress dependency of the drained compressibility, with higher modulus obtained under higher Terzaghi effective stress. The average drained bulk modulus values obtained are equal to 2985 MPa ( $\sigma_d = 14$  MPa) and 2027 MPa ( $\sigma_d = 12$  MPa) for tests EST31912c and EST31912e, respectively.

#### 4.4. Pore pressure loading test

Equation (9) shows that the Biot modulus  $H$  can be determined by running a test in which pore pressure is changed under constant total stress. Equation (9) also shows the relation between  $H$ ,  $b$ ,  $K_d$  and  $K_s$ . This test should be carried out under a slow rate of pressure change (0.5 kPa/mn), like in a drained test, to ensure uniform pore pressure distribution within the sample. The pore pressure was first increased from 4 MPa up to 4.8 MPa and then decreased, resulting in an unloading-reloading cycle in Terzaghi effective stress. As previously, the pressure change was chosen small enough to remain in the elastic domain and avoid any potential damage of the sample. As seen in Figure 9, the response is linear and anisotropic with smaller radial strains and an anisotropy ratio  $\varepsilon_1/\varepsilon_2$  of 1.8 and 1.5 for samples EST31912c and EST31912e, respectively.

Like in the drained test, one observes the stress dependency of the Biot modulus ( $H$ ) with respect to Terzaghi effective stress, with average values of 3470 MPa and 2237 MPa under 10 MPa and 8 MPa, respectively.

### 5. Analysis of experimental results and discussion

#### 5.1. Overall compatibility of the equivalent isotropic parameters

The compatibility of the set of equivalent isotropic poroelastic parameters determined from the various tests is now examined within the isotropic poroelastic framework presented in Section 2. This compatibility analysis is similar to that performed by Ghabezloo *et al.* (2008) on a set of poroelastic parameters of a hardened cement paste. The unjacketed modulus  $K_s$  directly evaluated from the unjacketed test ( $K_s = 21730$  MPa, see Figure 5) can also be calculated indirectly from the values of the drained bulk modulus ( $K_d$ ) and the Biot's modulus ( $H$ ) using equation (9). As seen in Table 2, the indirectly evaluated  $K_s$  values for both samples are very close to that measured in the unjacketed test. As expected, the values of  $K_d$  and  $H$  are stress dependent but they finally provide comparable (not stress dependent) values of  $K_s$ . This analysis shows the compatibility of the results of drained, unjacketed and pore pressure loading tests.

The Biot effective stress coefficient  $b$  can be determined by using the various poroelastic relations presented below ((31)-a to c) by combining the results of two tests among the four tests performed (drained, undrained, unjacketed compression and pore pressure loading tests).

Expressions (31)-d and (31)-e use the results of all tests to evaluate  $b$ . Note however that equations (c) and (d) cannot be used for sample EST31912e since the Skempton coefficient could not be measured.

$$b = \begin{cases} \frac{K_d}{H} & (a) \\ 1 - \frac{K_d}{K_s} & (b) \\ \frac{1}{B} \left( 1 - \frac{K_d}{K_u} \right) & (c) \\ \frac{K_u}{BK_u + H} & (d) \\ \frac{K_u(K_s - K_d)}{K_s(K_u - K_d) + H(K_s - K_d)} & (e) \end{cases} \quad (31)$$

The Biot effective stress coefficients  $b$  calculated using the various expressions (31) are given in Table 3. One can see a good compatibility between the values calculated that vary between 0.84 and 0.89 with an average value of 0.87 for sample EST31912c and between 0.90 and 0.91 with an average value of 0.91 for sample EST31912e. Again, good overall compatibility of the set of poroelastic parameters of the COx claystone determined from the distinct tests performed is observed, with a stress dependency of the  $b$  coefficient (0.87 under  $\sigma = 12$  MPa and 0.91 under  $\sigma = 12$  MPa). This analysis shows again the overall compatibility between all the experiments and provides confidence in the parameters determined. One can then calculate the Skempton coefficient for sample EST31912e, providing a value of 0.90 using relation (31)-c.

Based on the elastic parameters adopted by Gens *et al.* (2007) and Charlier *et al.* (2013) (Young modulus  $E = 4$  GPa and Poisson ratio  $\nu = 0.3$ ), an equivalent drained bulk modulus  $K_d = 3.3$  GPa in the case of isotropy could be calculated. Using equation (7), an equivalent  $b$  value of 0.85 is calculated using this value of  $K_d$  and the measured value of theunjacketed modulus  $K_s = 21.73$  GPa. In other words, the damage of a laboratory sample tend to over-estimate the  $b$  parameter. Knowing the value of  $K_s$ , a reasonable value of the  $b$  parameter could be obtained if the elastic parameters of the in-situ claystone are carefully determined.

## 5.2. Effects of anisotropy on the unjacketed modulus

Figure 5 showed a significant anisotropy in the response of the unjacketed test, with a ratio  $\varepsilon_1/\varepsilon_2$  of 5.7 indicating a compressibility perpendicular to bedding significantly larger than that parallel to bedding. This ratio is actually the highest one observed in all the tests carried out in this work.

The relation between the unjacketed modulus and the compressibility of the solid phase is complex in the case of composite materials and natural rocks made up of various minerals. The unjacketed modulus is an overall response depending on the one hand on the response in compression of the elementary particles and on the other hand, on the way particles are organised together, i.e on the fabric (or texture). It has been shown that most minerals (including quartz and calcite) exhibit a significant anisotropy with a dependence of the elastic modulus with respect to the direction (Bass 1995). This is suspected to be also true for clays platelets (and more particularly for the smectite phase) with a significant effect of adsorbed water molecules that should increase the compressibility when they are mobilised, i.e. when compression is carried out perpendicular to the platelet. Note that an isotropic overall response in unjacketed test with comparable axial and radial strains can be observed (Coyner 1984), in sandstone for instance, when elementary grains (with anisotropic response) can be randomly oriented within the rock fabric, thanks to their rounded shape. This is obviously not the case of the fabric of the COx claystone where calcite, quartz and other detritic grains are embedded in a clay matrix (50%). In this case, the anisotropic response of the solid phase that is mobilised during an unjacketed test results from the combined response of the clay matrix and of the embedded grains. The response of the matrix itself results from both the anisotropic response of the elementary clay platelets (mixed layered illite-smectite) and their preferred orientation along the bedding plane.

### 5.3. Effect of anisotropy on the Biot effective stress coefficient(s)

As shown in Section 2.2, the Biot  $b$  scalar coefficient defined in isotropic poroelastic media adopts a tensorial nature in transverse isotropic media, defined by two parameters  $b_1$  and  $b_2$  (Equations (17) and (18)).

In equations (23) to (30), one can see that the anisotropic ratio between the modulus measured along directions  $x_1$  and  $x_2$  for each test become equal if  $b_1 = b_2$ . However, the strain measurements made here through different experiments evidence some anisotropy that should affect the scalar nature of the  $b$  coefficient.

From equations (23) to (26), the Biot coefficients  $b_1$  and  $b_2$  can be written as a function of the measured parameters  $D_1$ ,  $D_2$ ,  $H_1$ ,  $H_2$  and of the unknown parameter  $\nu_{12}$ , as follows:

$$b_1 = -2\nu_{12} \left[ \left( \frac{\nu_{12}}{H_1} + \frac{1}{H_2} \right) / \left( \frac{\nu_{12}}{D_1} + \frac{1}{D_2} \right) \right] - (1 - 2\nu_{12}) \frac{D_1}{H_1} \quad (32)$$

$$b_2 = - \left[ \left( \frac{\nu_{12}}{H_1} + \frac{1}{H_2} \right) / \left( \frac{\nu_{12}}{D_1} + \frac{1}{D_2} \right) \right] \quad (33)$$

1  
2  
3  
4  
5  
6  
7  
8  
9  
10  
11  
12  
13  
14  
15  
16  
17  
18  
19  
20  
21  
22  
23  
24  
25  
26  
27  
28  
29  
30  
31  
32  
33  
34  
35  
36  
37  
38  
39  
40  
41  
42  
43  
44  
45  
46  
47  
48  
49  
50  
51  
52  
53  
54  
55  
56  
57  
58  
59  
60  
61  
62  
63  
64  
65

Table 4 summarizes the measured anisotropic moduli obtained from the drained compression and from the pore pressure test on samples EST31912c and EST31912e. The difference between the ratio  $D_2/D_1$  and  $H_2/H_1$  is also shown. Now, the estimation of  $b_1$  and  $b_2$  is only dependent of the unknown parameter  $\nu_{12}$ . The calculated values of  $b_1$  and  $b_2$  when  $\nu_{12}$  is varied between two values considered as reasonable boundaries (0.25 and 0.35) are presented in Table 5.

One can see that the calculated values of  $b_1$  and  $b_2$  for each experiment show a weak dependency with respect to the changes in  $\nu_{12}$ . Actually, the parameter  $\nu_{12}$  could be measured by a triaxial shearing test, not planned in the present experimental program carried out in an isotropic compression cell. Note however that Menaceur *et al.* (2015b) obtained a  $\nu_{12}$  value of 0.30 on the Callovo-Oxfordian claystone whereas Homand *et al.* (2006) provided a value of 0.35.

Adopting a value of 0.3 for  $\nu_{12}$  provides values of  $b_1 = 0.845$  and  $b_2 = 0.896$  under 10 MPa Terzaghi effective stress on specimen EST31912c and of  $b_1 = 0.870$  and  $b_2 = 0.976$  under 8 MPa on specimen EST31912e.  $b_i$  parameters are smaller under lower stress, but specimen EST31912e, with smaller degree of saturation, is probably more damaged, another reason of having a smaller  $b$  value (Aublivé-Conil 2003).

## 6. Conclusion

The values of the poroelastic parameters of the Callovo-Oxfordian claystone are still debated with published values of Biot coefficient comprised between 0.3 and 1.0, and an average value of 0.6 generally adopted in numerical simulations. To provide further information on parameters that are of great importance in the hydro-mechanical modelling in the close field around deep geological repository of radioactive waste, an experimental program was conducted in a specially designed isotropic compression cell. High precision strain measurements were made possible by getting rid of the parasite effects of the rubber membrane. To do so, direct contact through the membrane between the LVDTs stem and the specimen has been permitted, improving significantly the accuracy of the measurements of radial and axial strains. Great care was also devoted to the saturation procedure that was carried out under stress conditions close to in-situ, following previous works (Monfared *et al.*, 2011a, 2011b, 2012; Mohajerani *et al.*, 2013; Menaceur *et al.*, 2015a, 2015b) on low permeability claystones (Callovo-Oxfordian claystone and Opalinus clay) and the Boom clay. Satisfactory drainage conditions were also ensured by adopting a small drainage length (10 mm) and low enough stress rates during isotropic compression. The parasite effects of the drainage system on the measurement of undrained parameters have also been corrected.

1 Various poromechanical experiments have been performed: drained and undrained isotropic  
2 compression tests, unjacketed compression test and pore pressure loading test. The experimental  
3 results provided a direct determination of the equivalent isotropic poroelastic parameters of the  
4 COx claystone: drained bulk modulus  $K_d$ , undrained bulk modulus  $K_u$ , Skempton coefficient  $B$ ,  
5 unjacketed modulus  $K_s$  and Biot modulus  $H$ . A compatibility analysis has also been performed in  
6 the framework of linear isotropic poroelasticity. A very good compatibility was found between the  
7 results of various experiments, showing their good quality, demonstrating the robustness of the  
8 method and giving confidence in the experimental data obtained. The data showed the stress  
9 dependency of parameters  $K_d$ ,  $K_u$  and  $H$  that increased with increased effective stress. An indirect  
10 evaluation of the unjacketed modulus  $K_s$  showed that it was not stress dependent. For the tested  
11 specimens, cored at a depth of 490 m in the Underground Research Laboratory of Bure with around  
12 50% clay fraction, the value of the equivalent isotropic Biot effective stress coefficient was found  
13 equal to 0.91 under a stress state close to that prevailing in-situ (mean total stress of 12 MPa and  
14 pore pressure of 4 MPa).  
15  
16  
17  
18  
19  
20  
21  
22  
23

24 The COx claystone exhibited a well-marked transverse isotropic response under isotropic  
25 compression with axial strains smaller radial ones. An analysis in the framework of transverse  
26 isotropic poroelasticity provided the relations between the Biot effective stress coefficients  $b_1$  and  
27  $b_2$  and the Poisson's ratio  $\nu_{12}$  and the various moduli measured in the experiments. A parametric  
28 study showed that  $b_1$  and  $b_2$  had a very low sensitivity with respect to changes in  $\nu_{12}$ , allowing a  
29 reasonable estimation of  $b_1$  and  $b_2$  under the in-situ stress state with  $b_2$  (parallel to bedding) equal  
30 to 0.976, slightly higher than  $b_1$  (perpendicular to bedding), equal to 0.870. This difference is  
31 related to the mobilisation of the layers of water molecules adsorbed along the smectite faces in  
32 the mixed layer illite-smectite platelet within the clay matrix that results in a smaller stiffness  
33 perpendicular to bedding.  
34  
35  
36  
37  
38  
39  
40  
41  
42  
43

44 This work should be completed in the laboratory by poromechanical experiments under  
45 deviatoric loading to evaluate all the poroelastic parameters in the case of transverse isotropy. The  
46 variability and stress dependency of these parameters should also be studied.  
47  
48  
49

50 The poroelastic parameters determined here are that of a laboratory specimen previously  
51 extracted from the rock mass and probably affected by coring, stress release, desaturation,  
52 evaporation, trimming and resaturation under in-situ stresses. Given the susceptibility of  
53 claystones to damage, it is probable that these successive effects have some consequences on the  
54 parameters determined, like for instance an over-estimation of the  $b$  Biot parameter. In this regard,  
55  
56  
57  
58  
59  
60  
61  
62  
63  
64  
65

further investigation on the in-situ determination of the hydro-mechanical parameters of the claystone and the comparison of in-situ data with laboratory data remain necessary.

## **Appendix:**

### ***Correction of the effect of the drainage system in undrained tests***

The expression of the corrected Skempton coefficient ( $B^{cor}$ ) with respect to the measured one ( $B^{mes}$ ) is given below (Monfared *et al.*, 2011a). For the sake of simplicity the equations are written in terms of compressibility  $c_i = 1/K_i$ .

$$B^{corr} = \frac{B^{meas}}{1 + \frac{1}{V(c_d + c_s)} \left( V_p c_{dp} + V_g c_{dg} - B^{meas} \left( V_p (c_{dp} + \phi c_w) + V_g c_{dg} + V_L (c_w + c_L) \right) \right)} \quad (34)$$

The corrected undrained compressibility ( $c_u^{cor}$ ) is then written as:

$$c_u^{corr} = \frac{c_d - c_u^{meas}}{1 + \frac{1}{V(c_d + c_s)} \left( V_p c_{dp} + V_g c_{dg} - \left( V_p (c_{dp} + \phi_p c_w) + V_g c_{dg} + V_L (c_w + c_L) \right) \frac{c_d - c_u^{meas}}{c_d - c_s} \right)} \quad (35)$$

where  $V_p$ ,  $V_g$  and  $V_L$  are the volumes of the porous disk, geotextile and connecting lines, respectively and  $c_{dp}$ ,  $c_{dg}$  and  $c_L$  their drained compressibilities.  $\phi$  and  $\phi_p$  are the porosities of the sample and the porous disk respectively.  $V$ ,  $c_d$ ,  $c_u$ , and  $B$  are the volume, the drained compressibility, the undrained compressibility and the Skempton coefficient of the sample.  $c_s$  is the unjacketed compressibility.

The volume of samples EST31912c and EST31912e are  $V=11795 \text{ mm}^3$  and  $V=13847 \text{ mm}^3$ , respectively. The volume of the connecting lines, porous disk and geotextile are  $V_L=2412 \text{ mm}^3$ ,  $V_p=2268 \text{ mm}^3$  and  $V_g=113 \text{ mm}^3$ , respectively. Monfared *et al.* (2011a) performed a calibration test on a dummy metal sample and found a drained compressibility of the connecting lines  $c_L=0.32 \text{ GPa}^{-1}$ , a drained compressibility of the porous disk  $c_{dp}=1.02 \text{ GPa}^{-1}$ , and a drained compressibility of the geotextile  $c_{dg}=9.33 \text{ GPa}^{-1}$ . The porosity of the porous disk was  $\phi_p=0.22$ . The water compressibility at  $25^\circ\text{C}$  is  $c_w=0.447 \text{ GPa}^{-1}$  (Spang, 2002). The corrected undrained bulk modulus and Skempton coefficient presented in 4.2 are evaluated using these parameters.

#### **A-1- Parametric study on the induced errors**

A parametric study is presented here to better clarify the influence of various material and drainage system properties on the induced errors on different undrained parameters. The error on a quantity  $Q$  is evaluated as  $(Q_{measured} - Q_{corrected})/Q_{corrected}$ . The most influent parameters on the error

1 are the drained compressibility  $c_d$ , the porosity  $\phi$  and the volume ratio of the drainage system to  
2 the volume of the tested sample  $V_L/V$ . In this study, we take three values of the drained  
3 compressibility  $c_d$  more or less equivalent to the ones of the COx claystone ( $0.1 \text{ GPa}^{-1}$ ,  $0.3 \text{ GPa}^{-1}$   
4 and  $0.6 \text{ GPa}^{-1}$ ) and  $c_s = c_\phi = 0.05 \text{ GPa}^{-1}$ . The volume ratio  $V_L/V$  is taken equal to 0.21 which  
5 corresponds to our experiment, and to further analyse the effect of the dead volume, a second ratio  
6 of 0.05 is also taken. The porosity is varied from 0.03 to 0.45.  
7  
8  
9

10 Figure 10 shows the error on the measurement of the Skempton coefficient. When the rock  
11 is relatively highly compressible ( $c_d = 0.5 \text{ GPa}^{-1}$  and  $c_d = 0.3 \text{ GPa}^{-1}$ ), the range of error does not  
12 vary a lot between small and high porosities. A greater volume of the drainage system  
13 underestimates the Skempton coefficient ( $B$ ). The measured Skempton coefficient juggles between  
14 a slight underestimating and a slight overestimating when a geotextile is used. But with a lower  
15 compressibility, the error varies a lot as a function of the porosity. In fact, we can observe that for  
16 a volume ratio of 0.21 the Skempton coefficient is underestimated with an error of 44% in case of  
17 geotextile, for 0.03 porosity and it is overestimated with an error of 35% for 0.45 porosity. When  
18 a porous disk is used, the Skempton coefficient is always underestimated (from 65% to 22%) for  
19 the same volume ratio. The error is more important and  $B$  is highly overestimated if the volume  
20 ratio is smaller on the use of geotextile and a high porosity material.  
21  
22  
23  
24  
25  
26  
27  
28  
29  
30

31 The error made on the measurement of the undrained bulk modulus ( $K_u$ ) is shown on Figure  
32 11. Unlike for the Skempton coefficient, the error is more important for higher compressibilities.  
33 The effect of the volume ratio is more significant in the error on the measurement of  $K_u$ , as a large  
34 difference is shown between the two volume ratios. Once more, the error induced by the use of a  
35 porous disk is slightly more important than the geotextile.  
36  
37  
38  
39  
40

## 41 **References**

- 42  
43 Andra (2005) Synthesis argile: evaluation of the feasibility of a geological repository in  
44 argillaceous formation. < [http://www.andra.fr/download/site-principal/document/  
45 editions/266.pdf](http://www.andra.fr/download/site-principal/document/editions/266.pdf) >.  
46  
47  
48  
49 Aublivé-Conil N (2003) Modélisation du comportement mécanique des argiles raides avec prise  
50 en compte de l'endommagement : application aux argilites de l'Est. PhD thesis, Université de  
51 Cergy Pontoise.  
52  
53  
54  
55 Bass JD (1995) Elasticity of Minerals, Glasses, and Melts. In: Thomas JA (ed) Mineral physics  
56 and crystallography: a handbook of physical constants. American Geophysical Union, pp 45–  
57 63  
58  
59  
60  
61  
62  
63  
64  
65

- 1 Bemmer E, Longuemare P, Vincké O (2004) Poroelastic parameters of Meuse/Haute Marne  
2 argillites: effect of loading and saturation states. *Appl Clay Sci* 26:359–366.
- 3 Berryman JG (1992) Effective stress for transport properties of inhomogeneous porous rock.pdf.  
4 *J Geophys Res* 17409–17429.
- 5  
6  
7 Bishop AW (1976) The influence of system compressibility on the observed pore-pressure  
8 response to an undrained change in stress in saturated rock. *Géotechnique* 26:371–375.
- 9  
10  
11 Charlier R, Collin F, Pardoën B, Talandier J, Radu JP, Gerard P (2013) An unsaturated hydro-  
12 mechanical modelling of two in-situ experiments in Callovo-Oxfordian argillite. *Eng Geol*  
13 165:46–63.
- 14  
15  
16  
17 Cheng AH (1997) Material coefficients of anisotropic poroelasticity. *Int J Rock Mech Min Sci*  
18 34:199–205.
- 19  
20  
21 Chiarelli AS (2000) Étude expérimentale et modélisation du comportement mécanique de l'argilite  
22 de l'est. PhD thesis, Université Lille I.
- 23  
24  
25 Chiarelli AS, Shao JF, Hoteit N (2003) Modeling of elastoplastic damage behavior of a claystone.  
26 *Int J Plast* 19:23–45.
- 27  
28  
29 Coyner KB (1984) Effects of stress, pore pressure, and pore fluids on bulk strain, velocity, and  
30 permeability in rocks. PhD thesis, MIT.
- 31  
32  
33 Davy C a., Skoczylas F, Barnichon J-D, Lebon P (2007) Permeability of macro-cracked argillite  
34 under confinement: Gas and water testing. *Phys Chem Earth, Parts A/B/C* 32:667–680.
- 35  
36  
37  
38 Delage P, Le T-T, Tang A-M, Cui YJ, Li XL (2007) Suction effects in deep Boom clay block  
39 samples. *Géotechnique* 57:239–44.
- 40  
41  
42 Delage P, Menaceur H, Tang A-M, Talandier J (2014) Suction effects in deep Callovo-Oxfordian  
43 claystone Suction effects in deep Callovo-Oxfordian claystone. *Géotechnique Lett* 4:267–  
44 271.
- 45  
46  
47  
48 Detournay E, Cheng AH (1993) Fundamentals of Poroelasticity. Chapter 5 *Compr Rock Eng Princ*  
49 *Pract Proj Vol II, Anal Des Method*, ed C Fairhurst, Pergamon Press II:113–171.
- 50  
51  
52 Escoffier S (2002) Caractérisation expérimentale du comportement hydromécanique des argilites  
53 de Meuse Haute-Marne. PhD thesis, Institut National Polytechnique de Lorraine.
- 54  
55  
56  
57 Ewy RT (2015) Shale/claystone response to air and liquid exposure, and implications for handling,  
58 sampling and testing. *Int J Rock Mech Min Sci* 80:388–401.
- 59  
60  
61  
62  
63  
64  
65

- 1 Gaucher E, Robelin C, Matray JM, Négrel G, Gros Y, Heitz JF, Vinsot A, Rebours H,  
2 Cassagnabère A, Bouchet A (2004) ANDRA underground research laboratory: Interpretation  
3 of the mineralogical and geochemical data acquired in the Callovian-Oxfordian formation by  
4 investigative drilling. *Phys Chem Earth* 29:55–77.  
5
- 6 Gens A, Vaunat J, Garitte B, Wileveau Y (2007) In situ behaviour of a stiff layered clay subject  
7 to thermal loading : observations and interpretation. *Géotechnique* 207–228.  
8
- 9 Ghabezloo S, Sulem J (2010) Effect of the volume of the drainage system on the measurement of  
10 undrained thermo-poro-elastic parameters. *Int J Rock Mech Min Sci* 47:60–68.  
11
- 12 Ghabezloo S, Sulem J (2009) Stress dependent thermal pressurization of a fluid-saturated rock.  
13 *Rock Mech Rock Eng* 42:1–24.  
14
- 15 Ghabezloo S, Sulem J, Guédon S, Martineau F, Saint-Marc J (2008) Poromechanical behaviour of  
16 hardened cement paste under isotropic loading. *Cem Concr Res* 38:1424–1437.  
17
- 18 Gibson RE, Henkel DJ (1954) Influence of Duration of tests at Constant Rate of Strain on  
19 Measured “Drained” Strength. *Géotechnique* 4:6–15.  
20
- 21 Hill R (1952) The Elastic Behaviour of a Crystalline Aggregate.pdf. *Proc Phys Soc* 65:349–354.  
22
- 23 Homand F, Shao JF, Giraud A, Auvray C, Hoxha D (2006) Pétrofabrication et propriétés mécaniques  
24 des argilites. *Comptes rendus Géoscience* 338:882–891.  
25
- 26 Hoxha D, Giraud A, Homand F, Auvray C (2007) Saturated and unsaturated behaviour modelling  
27 of Meuse-Haute/Marne argillite. *Int J Plast* 23:733–766.  
28
- 29 Hu DW, Zhang F, Shao JF (2013) Experimental study of poromechanical behavior of saturated  
30 claystone under triaxial compression. *Acta Geotech* 31–36.  
31
- 32 Menaceur H (2014) Comportement thermo-hydro-mécanique et microstructure de l’argilite du  
33 Callovo-Oxfordien. PhD thesis, Université Paris Est.  
34
- 35 Menaceur H, Delage P, Tang A-M, Conil N (2015a) On the Thermo-Hydro-Mechanical Behaviour  
36 of a Sheared Callovo-Oxfordian Claystone Sample with Respect to the EDZ Behaviour. *Rock  
37 Mech Rock Eng* 6–8.  
38
- 39 Menaceur H, Delage P, Tang A-M, Conil N (2015b) The thermo-mechanical behaviour of the  
40 Callovo-Oxfordian claystone. *Int J Rock Mech Min Sci* 78:290–303.  
41
- 42 Mohajerani M, Delage P, Sulem J, Monfared M, Tang A-M, Gatmiri B (2012) A laboratory  
43 investigation of thermally induced pore pressures in the Callovo-Oxfordian claystone. *Int J  
44 Rock Mech Min Sci* 52:112–121.  
45  
46  
47  
48  
49  
50  
51  
52  
53  
54  
55  
56  
57  
58  
59  
60  
61  
62  
63  
64  
65

- 1  
2  
3 Mohajerani M, Delage P, Sulem J, Monfared M, Tang A-M, Gatmiri B (2013) The Thermal  
4 Volume Changes of the Callovo–Oxfordian Claystone. *Rock Mech Rock Eng* 47:131–142.  
5  
6 Monfared M (2011) *Couplages température-endommagement-perméabilité dans les sols et roches*  
7 argileux. PhD thesis, Université Paris-Est.  
8  
9 Monfared M, Delage P, Sulem J, Mohajerani M, Tang A-M, De Laure E (2011a) A new hollow  
10 cylinder triaxial cell to study the behavior of geo-materials with low permeability. *Int J Rock*  
11 *Mech Min Sci* 48:637–649.  
12  
13 Monfared M, Sulem J, Delage P, Mohajerani M (2011b) A Laboratory Investigation on Thermal  
14 Properties of the Opalinus Claystone. *Rock Mech Rock Eng* 44:735–747.  
15  
16 Noiret A, Giot R, Bemer E, Giraud A, Homand F(2010) Hydromechanical behavior of Tournemire  
17 argillites : Measurement of the poroelastic parameters and estimation of the intrinsic  
18 permeability by oedometric tests.  
19  
20 Pham QT, Vales F, Malinsky L, Nguyen M-D, Gharbi H (2007) Effects of desaturation–  
21 resaturation on mudstone. *Phys Chem Earth, Parts A/B/C* 32:646–655.  
22  
23 Skempton AW (1954) The pore-pressure coefficients A and B. *Géotechnique* 4:143–147.  
24  
25 Sultan N, Delage P, Cui YJ (2000) Comportement thermomécanique de l’argile de Boom.  
26 *Comptes Rendus l’Académie des Sci - Ser IIB - Mech* 328:457–463.  
27  
28 Tang A-M, Cui Y-J, Barnel N (2008) Thermo-mechanical behaviour of a compacted swelling clay.  
29 *Geotechnique* 58:45–54.  
30  
31 Thompson M, Willis JR (1991) A Reformulation of the Equations of Anisotropic Poroelasticity. *J*  
32 *Appl Mech* 58:612–616.  
33  
34 Valès F, Nguyen Minh D, Gharbi H, Rejeb A (2004) Experimental study of the influence of the  
35 degree of saturation on physical and mechanical properties in Tournemire shale (France).  
36 *Appl Clay Sci* 26:197–207.  
37  
38 Vincké O, Longuemare P, Boutéca M, Deflandre J-P (1998) Investigation of the poromechanical  
39 behavior of shales in the elastic domain. *Pap SPE* 47589 1–6.  
40  
41 Wan M, Delage P, Tang A-M, Talandier J (2013) Water retention properties of the Callovo-  
42 Oxfordian claystone. *Int J Rock Mech Min Sci* 64:96–104.  
43  
44 Wileveau Y, Cornet FH, Desroches J, Blumling P (2007) Complete in situ stress determination in  
45 an argillite sedimentary formation. *Phys Chem Earth* 32:866–878.  
46  
47  
48  
49  
50  
51  
52  
53  
54  
55  
56  
57  
58  
59  
60  
61  
62  
63  
64  
65

1  
2  
3  
4  
5  
6  
7  
8  
9  
10  
11  
12  
13  
14  
15  
16  
17  
18  
19  
20  
21  
22  
23  
24  
25  
26  
27  
28  
29  
30  
31  
32  
33  
34  
35  
36  
37  
38  
39  
40  
41  
42  
43  
44  
45  
46  
47  
48  
49  
50  
51  
52  
53  
54  
55  
56  
57  
58  
59  
60  
61  
62  
63  
64  
65

Wissa AEZ (1969) Pore pressure measurement in saturated stiff soils. *J Soil Mech Found Div Am Soc Civ Eng* 95 (SM4):1063–1073.

Yven B, Sammartino S, Geraud Y, Homand F, Villieras F (2007) Mineralogy, texture and porosity of Callovo-Oxfordian argillites of the Meuse/Haute-Marne region (eastern Paris Basin). *Mémoires la société Géologique Fr* 0249-7546:73–90.

Zhang CL (2011) Experimental evidence for self-sealing of fractures in claystone. *Phys Chem Earth* 36:1972–1980.

Zhang CL, Rothfuchs T (2004) Experimental study of the hydro-mechanical behaviour of the Callovo-Oxfordian argillite. *Appl Clay Sci* 26:325–336.

Zhang F, Xie SY, Hu DW, Gatmiri B (2012) Effect of water content and structural anisotropy on mechanical property of claystone. *Appl Clay Sci* 69:79–86.

Zimmerman RW (2000) Coupling in poroelasticity and thermoelasticity. 37:79–87.

Zimmerman RW, Somerton WH, King MS (1986) Compressibility of porous rocks. *J Geophys Res* 91:12765–12777.

## Figure captions

1 Figure 1. (a) Isotropic compression cell; (b) Overall system with controlled temperature bath

2 Figure 2. Displacement measurement system

3 Figure 3. Accuracy of strain measurement in contact with the rock

4 Figure 4. Saturation phase: (a) sample EST31912c, (b) sample EST31912e

5 Figure 5. Unjacketed test (EST31912-c), pressure-strain response in loading phase

6 Figure 6. Skempton coefficient measured for test EST31912c

7 Figure 7. Undrained isotropic compression tests: (a) EST31912c, (b) EST31912e

8 Figure 8. Drained isotropic compression cycles: (a) EST31912c, (b) EST31912e

9 Figure 9. Pore pressure loading-unloading test: (a) EST31912c, (b) EST31912e

10 Figure 10. Parametric study of the error on Skempton coefficient ( $B$ )

11 Figure 11. Parametric study of the error on the undrained modulus ( $K_u$ )

## Table captions

- 1 Table 1. Initial characteristics of the studied specimens
- 2
- 3 Table 2. Calculated  $K_s$  from measured  $K_d$  and  $H$ .
- 4
- 5 Table 3. Calculation of the Biot effective stress coefficient  $b$ .
- 6
- 7 Table 4. Measured anisotropic modulus in drained and pore pressure tests.
- 8
- 9 Table 5. Calculation of  $b_1$  and  $b_2$  for different  $v_{12}$ .

10  
11  
12  
13  
14  
15  
16  
17  
18  
19  
20  
21  
22  
23  
24  
25  
26  
27  
28  
29  
30  
31  
32  
33  
34  
35  
36  
37  
38  
39  
40  
41  
42  
43  
44  
45  
46  
47  
48  
49  
50  
51  
52  
53  
54  
55  
56  
57  
58  
59  
60  
61  
62  
63  
64  
65

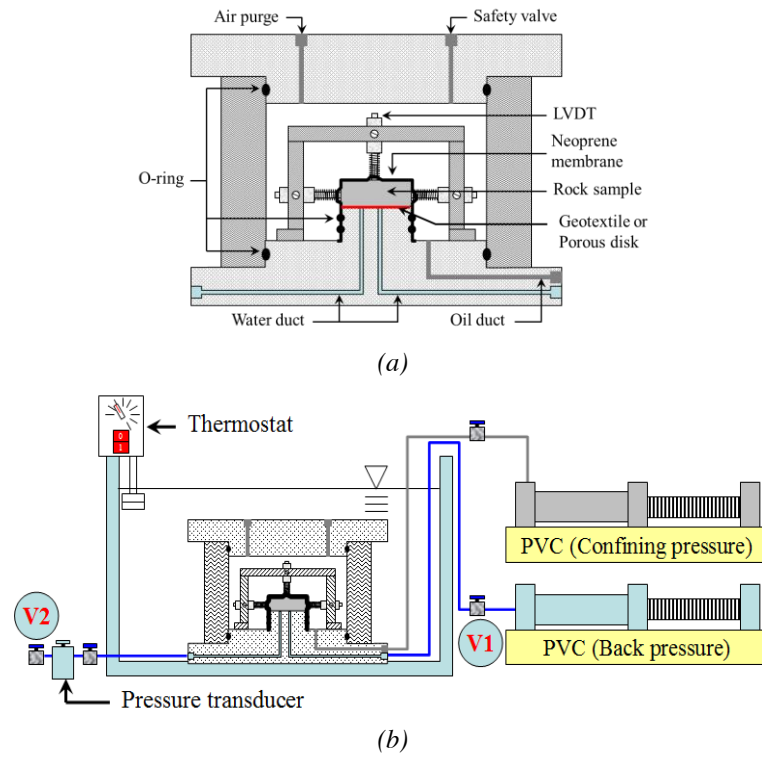
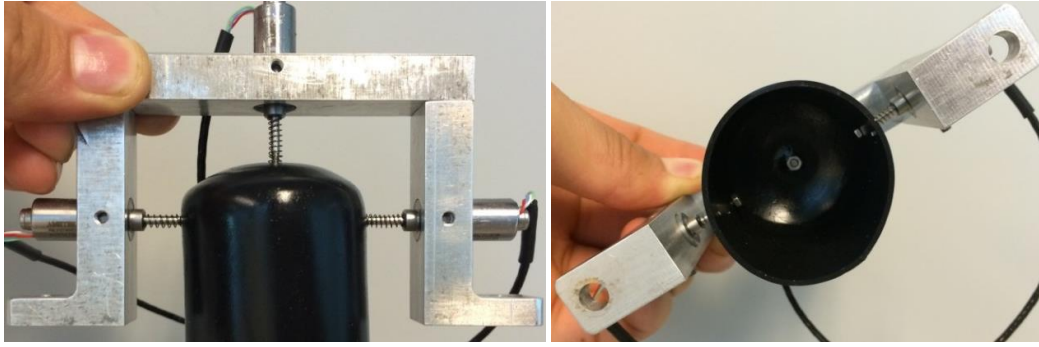


Figure 1. (a) Isotropic compression cell; (b) Overall system with controlled temperature bath



*Figure 2. Displacement measurement system*

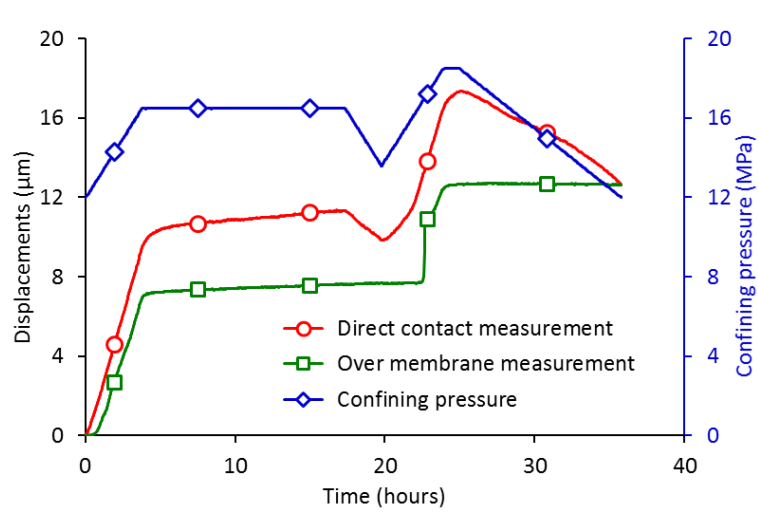


Figure 3. Accuracy of strain measurement in contact with the rock.

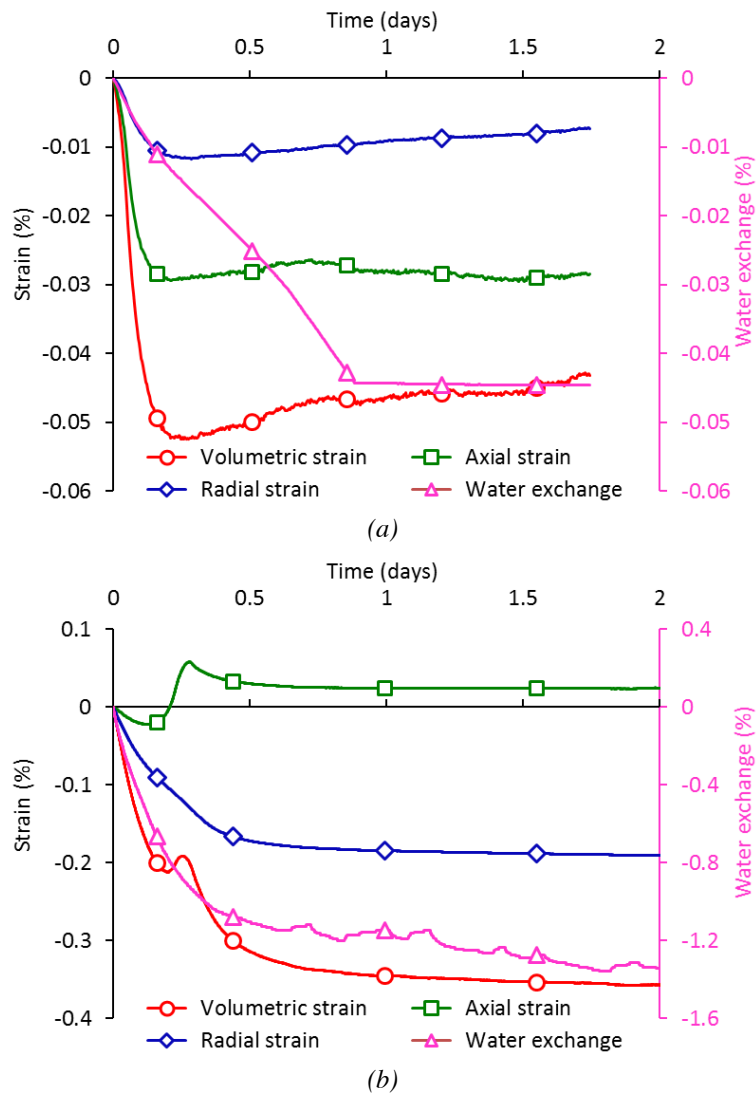


Figure 4. Saturation phase: (a) sample EST31912c, (b) sample EST31912e.

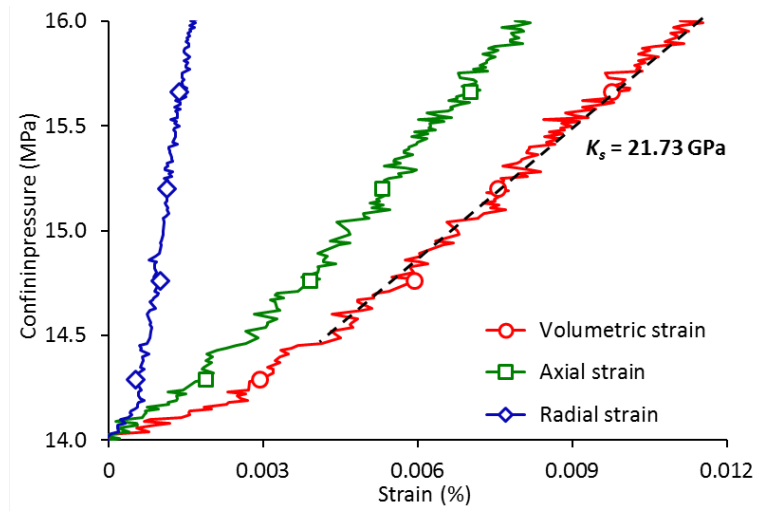


Figure 5. Unjacketed test (EST31912-c), pressure-strain response in loading phase

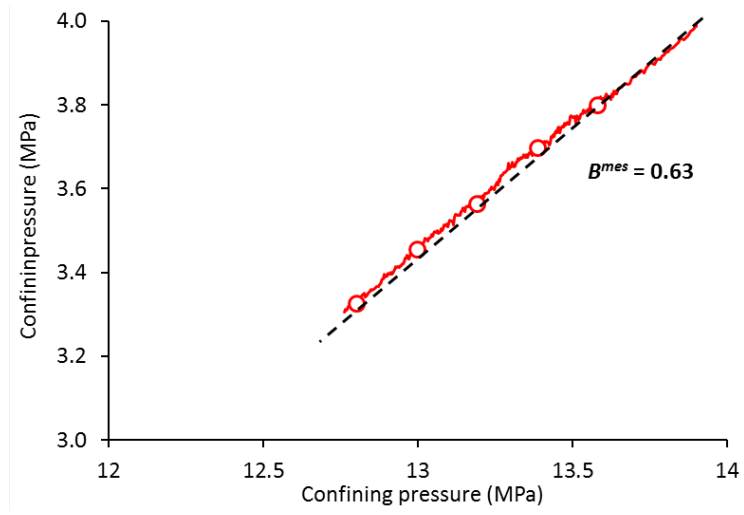


Figure 6. Skempton coefficient measured for test EST31912c

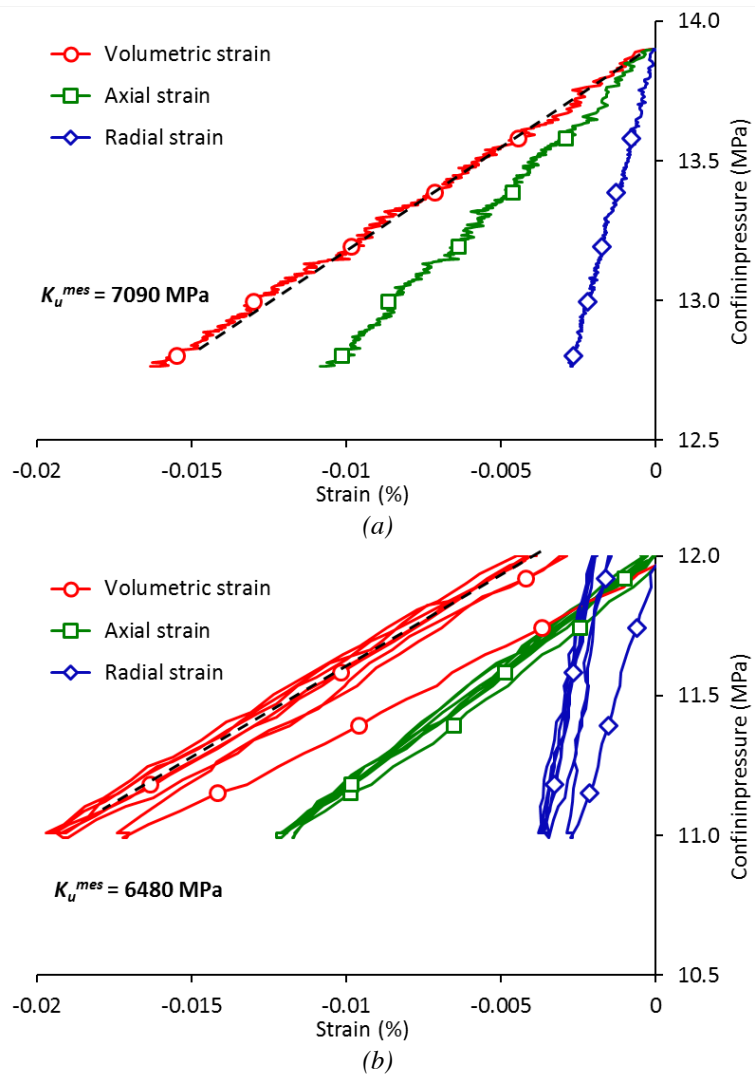
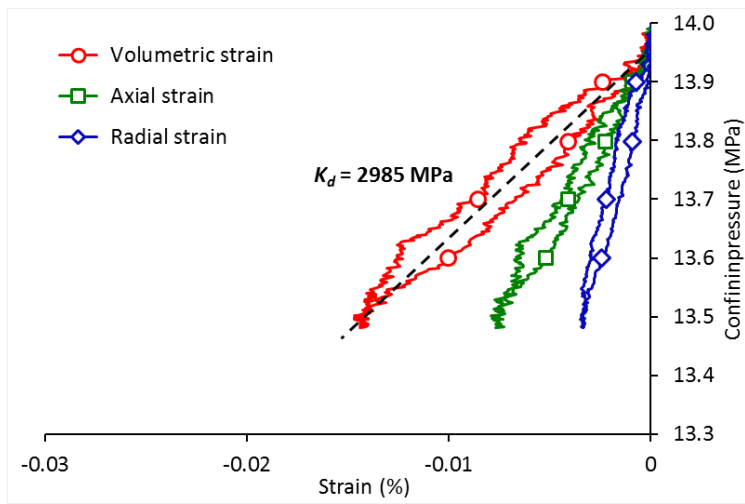
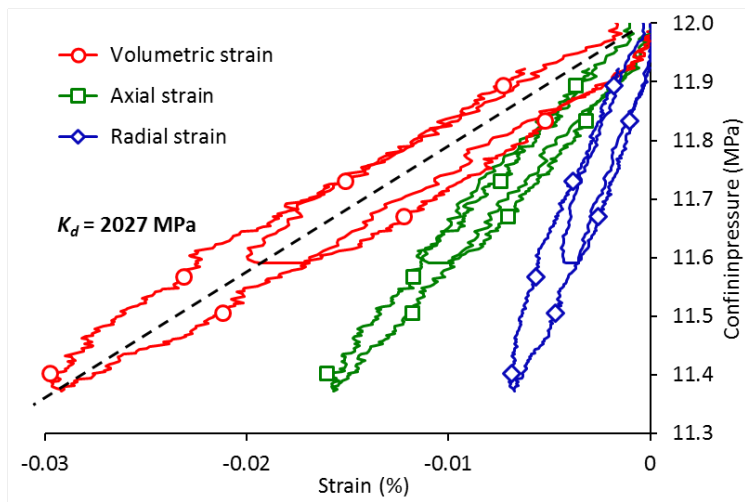


Figure 7. Undrained isotropic compression tests: (a) EST31912c, (b) EST31912e.



(a)



(b)

Figure 8. Drained isotropic compression cycles: (a) EST31912c, (b) EST31912e.

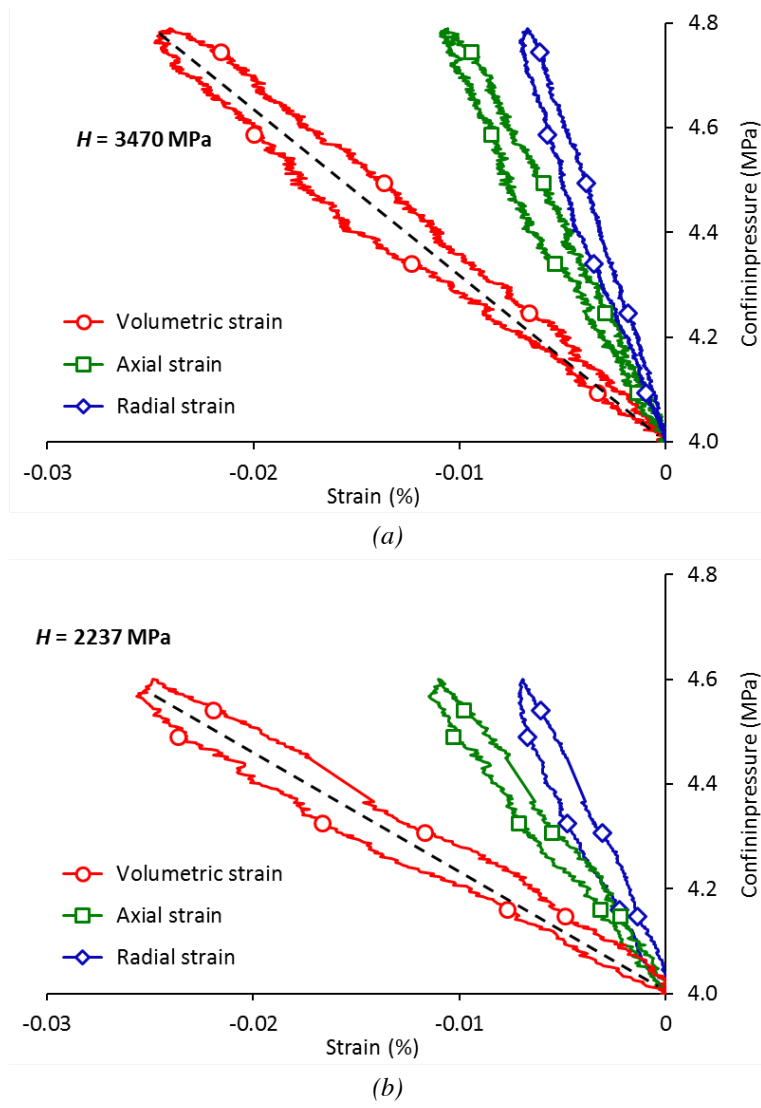


Figure 9. Pore pressure loading-unloading test: (a) EST31912c, (b) EST31912e.

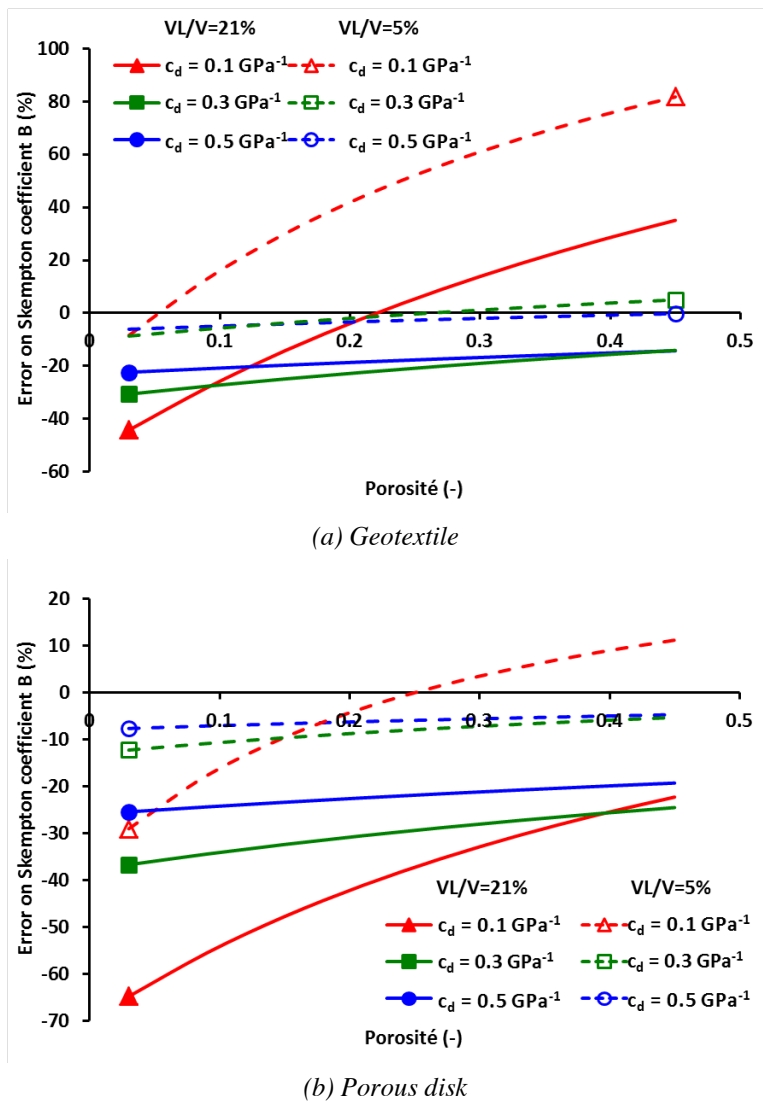
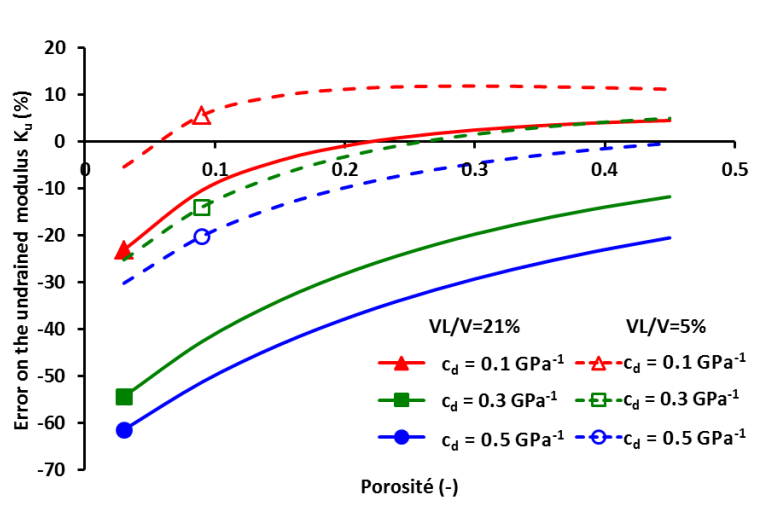
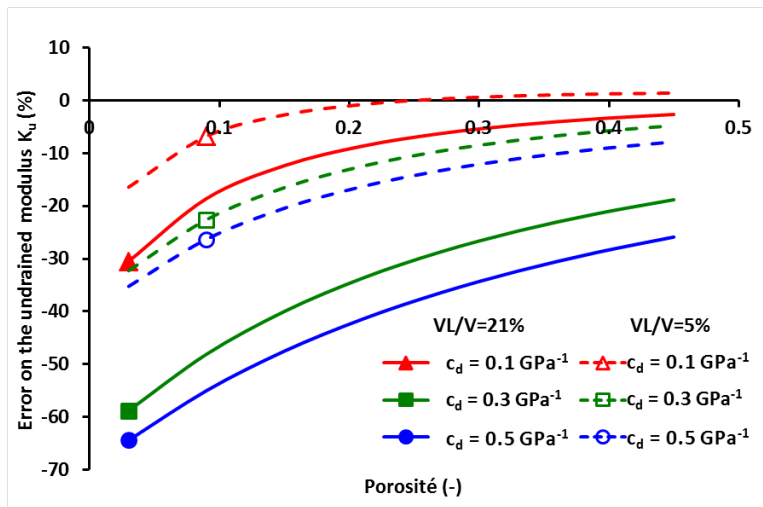


Figure 10. Parametric study of the error on Skempton coefficient (B)



(a) Geotextile



(b) Porous disk

Figure 11. Parametric study of the error on the undrained modulus ( $K_u$ )

*Table 1. Initial characteristics of the studied specimens*

ID Ech.	$w$ (%)	$\rho$ (g/cm <sup>3</sup> )	$\rho_d$ (g/cm <sup>3</sup> )	$e$	$S_r$ (%)	$\phi$ (%)	Suction (MPa)
EST31912c	7.45	2.39	2.22	0.21	94.2	17.6	19.7
EST31912e	4.54	2.39	2.29	0.18	67.8	15.3	-

*Table 2. Calculated  $K_s$  from measured  $K_d$  and  $H$ .*

	EST31912c ( $\sigma_d = 10$ MPa)	EST31912e ( $\sigma_d = 8$ MPa)
Measured $K_d$ (Figure 8)	2985 MPa	2027 MPa
Measured $H$ (Figure 9)	3470 MPa	2237 MPa
Calculated $K_s$	21357 MPa	21592 MPa
Measured $K_s$ (Figure 5)	21730 MPa	

Table 3. Calculation of the Biot effective stress coefficient  $b$ .

		EST31912c ( $\sigma_d = 10$ MPa)	EST31912e ( $\sigma_d = 8$ MPa)
Unjacketed modulus $K_s$		21730 MPa	
Drained modulus $K_d$		2985 MPa	2027 MPa
Biot modulus $H$		3470 MPa	2237 MPa
Undrained modulus $K_u$		12424 MPa	10931 MPa
Skempton coefficient $B$		0.84	-
Biot's coefficient $b$	(a)	0.86	0.91
	(b)	0.85	0.90
	(c)	0.91	-
	(d)	0.89	-
	(e)	0.86	0.91
Mean Biot coefficient $b$		0.87	0.91

*Table 4. Measured anisotropic modulus in drained and pore pressure tests.*

	EST31912c ( $\sigma_d = 10MPa$ )	EST31912e ( $\sigma_d = 10MPa$ )
$D_1$ (GPa)	5.6	3.7
$D_2$ (GPa)	12.8	9
$H_1$ (GPa)	-7.3	-5.2
$H_2$ (GPa)	-13	-7.7
$D_2/D_1$	2.3	2.4
$H_2/H_1$	1.8	1.5

*Table 5. Calculation of  $b_1$  and  $b_2$  for different  $\nu_{12}$ .*

$\nu_{12}$	EST31912c ( $\sigma_d = 10$ MPa)		EST31912e ( $\sigma_d = 8$ MPa)	
	$b_1$	$b_2$	$b_1$	$b_2$
0.25	0.836	0.906	0.854	0.996
0.3	0.845	0.896	0.870	0.976
0.35	0.852	0.888	0.884	0.959